JOURNAL OF MATERIALS SCIENCE 27 (1992) 3341–3352

Structural characteristics of a nickel-modified Al–20Si–3Cu–1Mg alloy powder

J. ZHOU, J. DUSZCZYK, B. M. KOREVAAR
Laboratory for Materials Science, Delft University of Technology, Rotterdamseweg 137, 2628 AL Delft, The Netherlands

An attempt has been made to characterize a new, complicated Al–20Si–7.5Ni–3Cu–1Mg alloy powder produced by air atomization as a means of rapid solidification and its structural evolutions during continuous heating, in order to provide basic information for further investigations on its deformation behaviour and properties. The characterization consisted of size measurements, morphological observations, structural and thermal analyses of bulk powder, and microstructural examinations of individual powder particles. It was observed that the powder had a wide size distribution and irregular shapes, which were closely related to its varying internal structures. X-ray diffractometry (XRD) showed little shift of the diffraction line from the aluminium matrix of the powder, but a significant broadening, which has been attributed partly to the non-uniformity of supersaturation in the matrix of the powder and partly to the strains caused by the silicon crystals in the material. A differential scanning calorimetry (DSC) analysis revealed complex decomposition behaviour of the meta-stable aluminium matrix and transformations of nickel-bearing intermetallic compounds when heat was applied to the powder. XRD also showed that the meta-stable compounds formed in the powder did not match any known phases, and that they were transformed into Al_3Ni, $Al_3(NiCu)_2$ and Al_7Cu_4Ni intermetallic dispersoids upon heating. The analyses also indicated that, due to the addition of nickel, some copper-containing phases, initially desired to create precipitation strengthening effects, no longer existed. This would diminish the ageing response of the alloy and probably change its category to be non-heat treatable – an important modification that has not yet been recognized by the alloy designers and users. Examinations on the powder particle sections showed variations in microstructure with powder particle size. Transitions in solidification mode within powder particles in accordance with local conditions of undercooling and heat extraction were also observed. The significant inhomogeneities in the microstructure of the powder have raised a problem to which special attention should be paid in both powder production and subsequent processing.

1. Introduction

One of the most important properties of hypereutectic Al–Si alloys, which makes them unique and attractive to the manufacturers of engines and compressors, is their high dimensional stability in response to temperature changes, which is reportedly comparable with that of iron alloys [1]. Their low thermal expansion coefficients are basically attributed to the dispersion of a high volume fraction of silicon crystal phase in the aluminium matrix [2–4]. In order to improve their mechanical properties, high temperature strength in particular, a modification in composition is necessarily made by adding a transition element, very often iron, to an Al–Si base alloy [5]. In this case, the thermal expansion coefficient of the modified alloy is additionally affected by the intermetallic phases formed, as a direct result of a change in phase constituents. With a 5 wt % iron addition to the Al–20Si alloy, a high volume fraction of a meta-stable Al–Si–Fe compound (δ-Al_4FeSi_2 phase) is formed during rapid solidification, and then transformed into an equilibrium Al–Si–Fe compound (β-Al_5SiFe) during further processing. As a result of the Al–Si–Fe intermetallic compound formation, the relative volume fraction of free silicon crystals is reduced. This is consistent with the observation of a faceted/non-faceted eutectic appearance of the as-solidified structure in the Al–20Si–5Fe alloy produced by the Osprey process [6]. It has also been found that the balance between the reduction in the volume fraction of the free silicon crystals and the presence of the β-phase with a low thermal expansion coefficient makes the over-all thermal expansion coefficient of the Al–20Si–5Fe–3Cu–1Mg alloy remain similar to that of the Al–Si–Cu–Mg base alloy [7, 8], but the former possesses a markedly improved hot strength. This finding has provided the iron-modified Al–20Si–3Cu–1Mg alloy with the prospect of commercial adoption [9]. By now, a number of investigations on this iron-modified alloy have been conducted [10–12].

A desire to reduce the thermal expansion coefficient

0022–2461

of Al–Si–Cu–Mg based alloy further has recently led to a new choice of a transition element to be added. Nickel, having as low a diffusion coefficient in aluminium solid solution as iron, is known for tending to form Al–Ni binary compounds in the Al–Ni–Si ternary system [13]. This suggests that the addition of nickel may result not only in improving the hot strength of the base alloy, but also in lowering its thermal expansion coefficient, because a part of the aluminium is bound to form Al–Ni intermetallic compounds with low thermal expansion coefficients and the volume fraction of the free silicon crystals can be relatively increased. Previous measurements have verified this consideration, showing that the Al–20Si–3Cu–1Mg alloy with an addition of 7.5 wt % nickel possesses the same hot strength as that with an addition of 5 wt % iron, but the thermal expansion coefficient of the former is reduced by 15% [7–9]. This verification has become one of the main reasons for involving nickel in a number of newly designed Al–Si alloys subjected to research and production [14, 15]. Obviously, the addition of nickel poses new questions concerning the modifications in the as-solidified structures and their developments at each step of processing, which will undoubtedly affect the final structure and properties of the material. No detailed work has, however, been reported on the Al–Si–Ni–Cu–Mg quinary alloy, although the interest in using this alloy to make vanes in automotive air-conditioning compressors and plastics injection moulds has been aroused for nearly two years [16]. Investigating the complexity of this alloy in its fundamental aspects still remains a challenge.

The main purposes of the present investigation, as the first part of a comprehensive research programme, were to characterize the initial structures of the Al–20Si–7.5Ni–3Cu–1Mg alloy powder produced by air atomization and to examine the decomposition behaviour of the rapidly solidified material during a continuous heating process. The information obtained was intended to be used as a guide in determining an appropriate condition for the consolidation of the powder and understanding its structural development during subsequent processing.

2. Experimental procedure

The powder of the alloy, with a nominal composition of 20 wt % Si, 7.5 wt % Ni, 3 wt % Cu, 1 wt % Mg and balance aluminium, was produced using a commercial scale air atomizer at the Showa Denko KK in Japan. A chemical analysis of the atomized powder by means of atomic absorption spectrophotometry showed the exact composition of the alloy to be 19.3 wt % Si, 7.57 wt % Ni, 3.24 wt % Cu, 1.18 wt % Mg and balance aluminium. As a result of the oxidation during atomization in an oxidizing medium, the powder contained 0.22 wt % oxygen, as determined by means of a Stroehlein OSA–MAT apparatus. Auger spectroscopy revealed the average thickness of an oxide layer on the powder particle surfaces to be about 30–33 nm [17].

The size and size distribution of the powder in the dry state were measured using a Malvern laser particle sizer. Its morphological and topographical features were observed using scanning electron microscopy (SEM) and optical microscopy. Microstructural examinations were carried out on sections of the powder particles with various sizes. The section surfaces were deeply etched in a modified Keller and Wilcox's reagent and covered with a thin film of gold or carbon to obtain topographic contrast in SEM. The distributions of the alloying elements on polished powder particle sections were revealed by X-ray mapping. The compositional analyses of the as-solidified phases were performed by means of X-ray energy dispersive spectrometry (EDS) linked to SEM. The determination of the average lattice parameter of the as-solidified matrix and the identification of the phases formed in the atomized and heated powder were made by using X-ray powder diffractometry. A Siemens diffractometer with a stepping-motor driving system was employed. Copper radiation at 45 kV and 30 mA was selected and the analyses were done at 24 °C. Specimens were prepared by depositing a very thin layer of the powder particles on a silicon monocrystal substrate with an orientation of ⟨5 1 0⟩. DSC was carried out to investigate the decomposition behaviour of the powder during a slow heating process (5 °C min^{-1}) in a Du Point 9900 instrument. The powder weighing 32 mg was fed into a pan and the pan was then roughly sealed. A pure aluminium piece with a similar weight was used as a reference. In order to minimize the oxidation of the powder with its very large surface area (0.18 $m^2 g^{-1}$) during heating cycles, which would disturb the revelation of thermal reactions of interest, the specimen chamber was evacuated for about half an hour and then purged with argon for another half an hour prior to heating. The analysis was then performed in an argon atmosphere. Three heating cycles, followed by the cooling at different rates, were run to observe the changes in its thermal effects.

3. Results and discussion

3.1. General characteristics of the powder

Fig. 1 shows the size distribution of the powder. It was measured that, though the size had a wide span of 6–262 μm, 75% of the powder particles fell into a size band of 30–160 μm. The mass median size was about 65 μm. Understanding this characteristic is of importance, because, as will be shown later, the microstructures of the powder particles within the most populated size band are very different from each other. It means that the mechanisms operating during solidification are very sensitive to droplet size. The varying powder particle size is a major source of inhomogeneities in the as-solidified structure, which are possibly inherited by the final products. Unfortunately, the inhomogeneities in the starting material, the atomized powder, cannot be eliminated by applying a sieving process, otherwise the yield of the powder production will be too low to be allowed for commercial reasons.

Figs 2 and 3 show the SEM and optical morphologies of the powder, respectively. It can be seen from Fig. 2 that the shape of the powder particles is

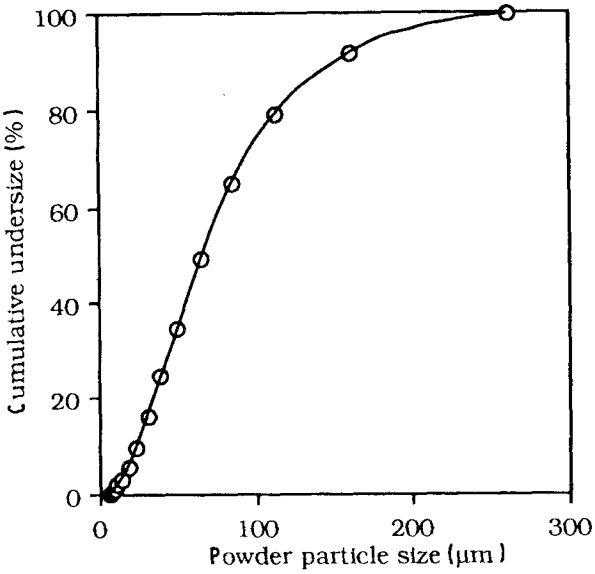

Figure 1 Size distribution of the powder particles, mass median size is 65.4 μm.

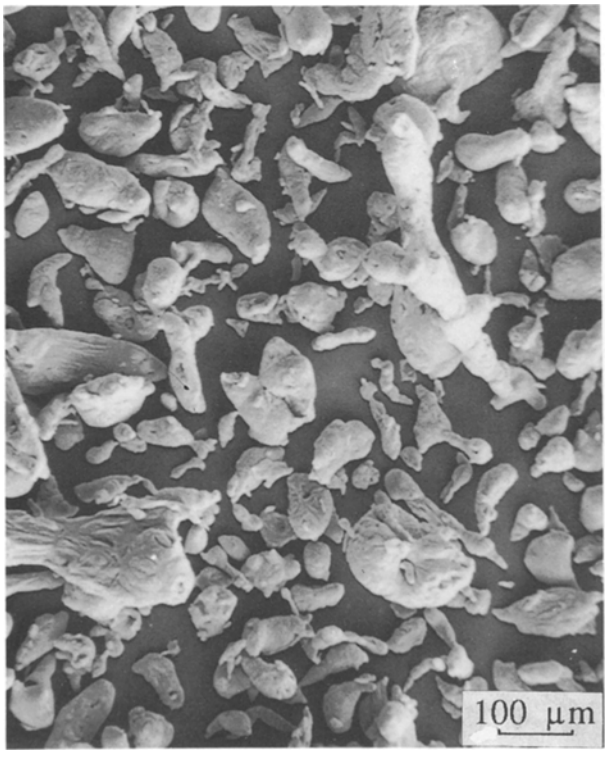

Figure 2 SEM morphology of the powder particles.

highly irregular, which clearly demonstrates the severity of oxidation occurring in the atomizing chamber with an oxidizing atmosphere which effectively prevented the spheroidization of the atomized droplets. The sections of the powder particles, Fig. 3, appear to exhibit less irregularity in their shape, revealing a teardrop shape of many powder particles, typical of those atomized in air. It is interesting to see pores in a number of powder particle sections. They may result from the random sectioning of the powder particles with an irregular morphology. However, another possibility that the atomizing gas is entrapped in those powder particles may also exist [18]. It is suggested

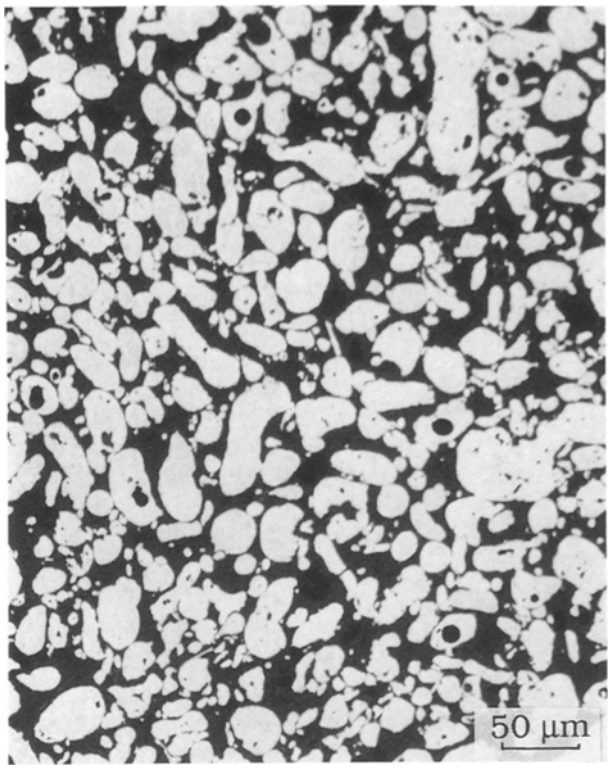

Figure 3 Optical morphology of the powder particle sections.

that, if this is really the case, imposing large deformation to the powder should be essential for the complete closure of the pores. Otherwise, a sound structure cannot be ensured when the material is subjected to further processing or being used at high temperatures where the evolution of the entrapped gas tends to occur. It should also be mentioned that the observed high irregularity in shape can help attain good interlocking between the powder particles [19], which is important for the cold precompaction of the powder prior to degassing and extrusion.

Of considerable interest is the topography of the powder particles. It was observed that finer powder particles generally had smoother surfaces. There can be a number of factors to account for this observation. First, the finer particles have higher driving forces to reduce their surface energies. The second factor can be smaller volume changes resulting from solidification shrinkage. The third factor is related to the type and the size of the as-solidified structure. Fig. 4 shows a part of a large powder particle, from which the evidence of solidification patterns due to shrinkage is visible, although the volume shrinkage of the present alloy should be considerably reduced by its very high silicon content. Also observable are a few very fine holes with a size of 0.5 μm in the powder particle surface (Fig. 4). It is generally understood that during atomization solidification starts at the droplet surface and proceeds toward the interior. This understanding raises the question: "where does final solidification shrinkage takes place?". The present observation suggests that the solidification may also end at the powder particle surface. For very fine powder particles with a single solidification event, the radial growth of solidification shows that the solidification proceeds

Figure 4 Topography of a powder particle showing an uneven surface.

from one side of the surface with a potent catalytic nucleus across their interior to the opposite [20]. For coarser powder particles, multiple nucleation events occur not only at their periphery but also at their interior. The final solidification does not necessarily occur in the interior, but may also occur at the surface. The observed holes in the depressed areas of the powder particle surface are very likely the locations where the final solidification occurred and the remainder of the liquid was drawn in.

3.2. Structural characteristics of bulk powder and their changes during heating

The structural information obtained from the bulk of the powder should be of use for getting an insight into the varying microstructures of individual powder particles. The X-ray diffraction line obtained from the reflection plane {442} of the aluminium matrix showed a considerable broadening (Fig. 5), which clearly indicates the existence of structural distortions in the matrix of the powder. Another important feature of the diffraction line observed was that the reflections from the K_{α_1} and K_{α_2} did not split. When the K_{α_2} component was excluded, it was found that the peak of the K_{α_1} reflection lay at a diffraction angle very close to that of pure aluminium, seemingly indicative of an unchanged average lattice parameter of the matrix in the powder. It is of great importance to note that the unchanged average lattice parameter found in the present alloy does not necessarily mean that the full precipitation of the solutes occurred in the atomized powder. It, on the contrary, implies that the presence of a volume fraction of the silicon crystal phase that is known for exerting tensile stresses on the aluminium matrix [21], together with the dissolved magnesium, counteracted the reduction of the matrix lattice size resulting from the supersaturation of silicon, nickel, and copper [13]. The evidence to support this argument is: after the hot consolidation of the powder in which most of the supersaturated atoms had precipitated out, an increased average lattice parameter was measured. This increase is largely due to the influence of the silicon crystal phase on the lattice size of the aluminium matrix, which has been repeatedly observed in Al–Si based alloys [6, 21]. It should also be pointed out that although the bulk of the powder showed an unchanged average lattice parameter, a significant variation of the parameter within and between the powder particles can be ex-

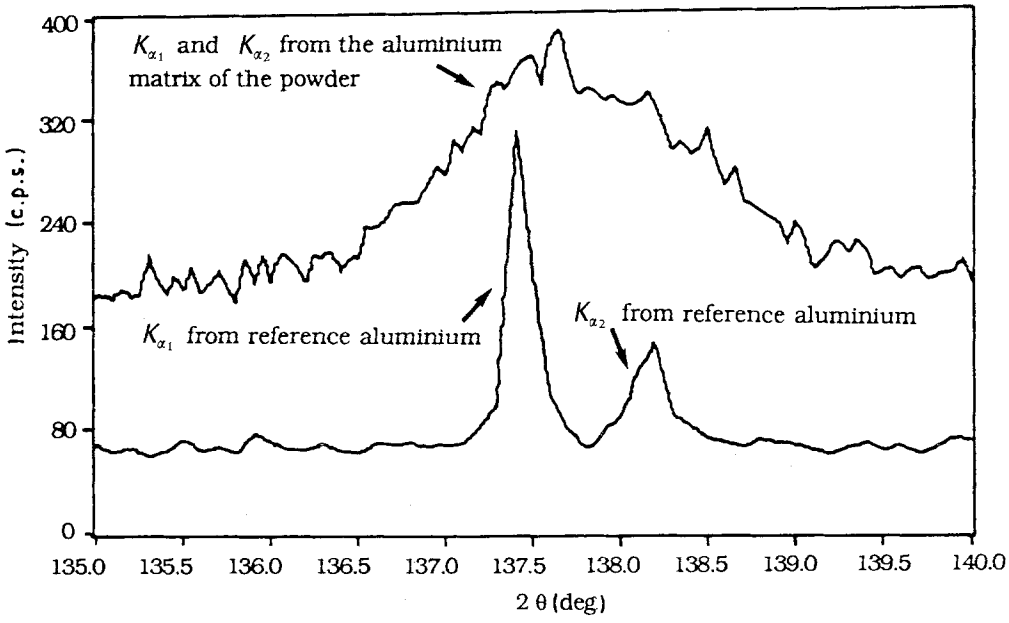

Figure 5 X-ray diffraction line from the aluminium matrix of the powder, reflection plane {422} using CuK_α radiation.

pected, as evidenced by the significant broadening of the diffraction line [22]. This is understandable because the matrix lattice parameter is basically affected by two factors in the Al–Si based alloys. The first is the entrapment of the solutes which, in the present alloy, give inconsistent impacts on the matrix lattice size. The second is a distribution of silicon crystals, which tends to increase the matrix lattice size. Both of these two factors are in turn dependent upon the undercooling and heat-releasing conditions that are principally a function of powder particle size. The bulk of the powder with a wide size range, as shown earlier, is likely to contain the meta-stable matrix with varying lattice sizes, as reflected by the asymmetric spreading of the reflection peak angle from the matrix of the powder as a whole. This explanation is supported by the observed wide variations in microstructure within and between the powder particles, which will be shown later.

Strong reflections from the silicon crystal phase, which has been considered to influence the matrix lattice parameter, were indeed detected from the atomized powder. A slight shift and broadening of the diffraction lines were observed, a phenomenon also reported in melt-spun Al–Si binary alloys [23]. It seems very unlikely that an appreciable amount of the other alloying atoms would be entrapped in the silicon crystals to result in the observed shift and broadening. A more likely cause are the microstrains in the silicon crystals, owing to the difference in thermal shrinkage between the silicon crystals and matrix, which would occur when the powder was cooled from solidification temperatures. The rest of the reflections detected in the X-ray diffraction analysis could not be assigned to any established compounds possibly formed in the Al–Si–Ni–Cu–Mg system, suggesting that the intermetallic phases formed in the powder were of non-equilibrium composition and structure. These meta-stable phases were transformed during subsequent heating into Al_3Ni, $Al_3(NiCu)_2$, and Al_7Cu_4Ni intermetallic compounds, which were definitely identified by X-ray diffraction and will be discussed at length in a forthcoming paper on the structural development during the hot consolidation of the powder.

As argued above, the matrix lattice parameter determined by X-ray diffraction is not a direct measure of the supersaturation in the as-solidified matrix of the powder. The supersaturation was, however, clearly revealed by the DSC runs. Several overlapping thermal reactions associated with the decomposition of the meta-stable aluminium matrix and the transformation of the meta-stable intermetallic phases occurred in the powder when the atomized powder was heated. Fig. 6 presents the recorded DSC traces of three heating cycles. Obviously, the decomposition behaviour of the atomized powder under study is more complex than that of the Al–Si–Cu–Mg base alloy powder, of which the DSC curves are also given in the thermograph for comparison. At least three major exothermic effects from the present powder are apparent from the trace of the first heating cycle in the thermograph. The first one centred at 206 °C is most likely caused by the precipitation of silicon from the meta-stable aluminium matrix and probably also by the morphological changes of the silicon phase, resulting in a reduction in system energy. This thermal effect has been observed in a number of the analyses of rapidly solidified Al–Si binary alloys [24, 25]. The area bounded by the peak, representing the amount of energy released from the present powder, is, however, small as compared with the results obtained from other Al–Si based alloys produced by water atomization, single and twin roller techniques [26, 27]. One

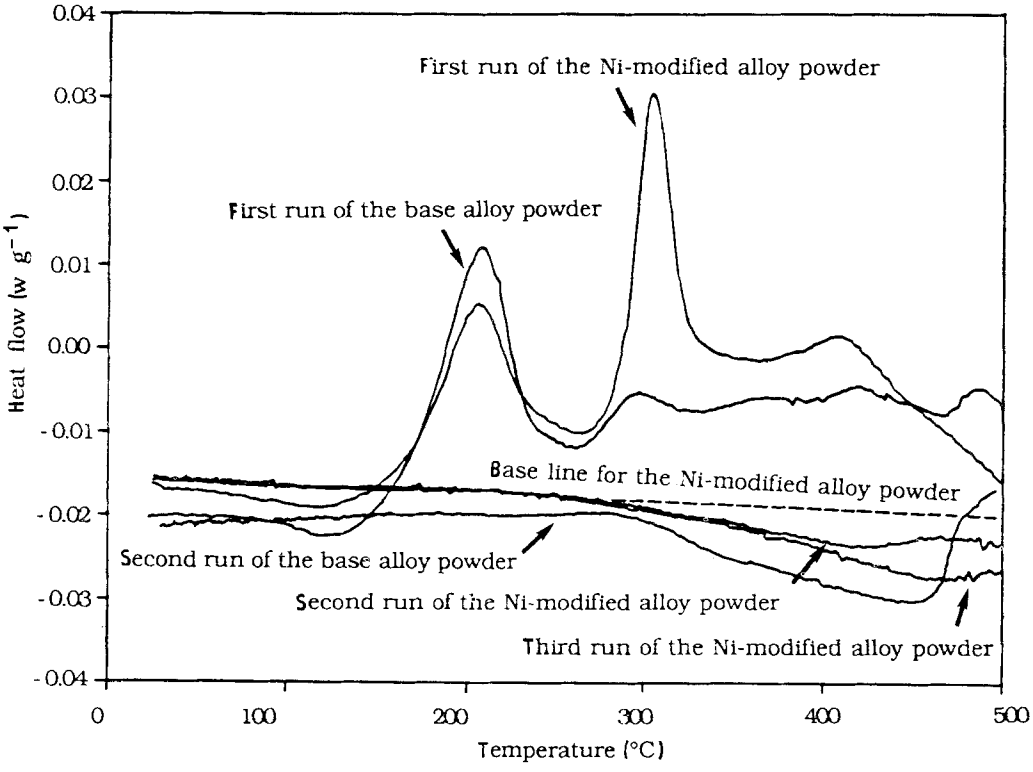

Figure 6 DSC thermograph of the nickel-modified alloy powder in comparison with that of the base alloy powder.

of the main reasons can be that the cooling rates achieved in the air atomization, which principally determine the degree of silicon supersaturation in the aluminium matrix, are lower than those in the other techniques. Another factor which should be taken into consideration is the addition of 7.5 wt % nickel to the Al–Si–Cu–Mg base alloy that leads to a reduction of the silicon solubility in the aluminium matrix [13]. This explanation is supported by the fact that the base alloy powder without the nickel addition, produced under identical conditions, showed a higher energy release from this exothermic reaction, as shown in Fig. 6.

The second large peak exhibited by the nickel-modified alloy powder during the first heating cycle, over the temperature range 250–380 °C (extrapolated down to the dashed base line in Fig. 6), is ascribed to the evolution of a nickel-containing compound from a meta-stable form to an equilibrium one. This consideration is first based on the comparison in thermal effects between the base and modified alloy powders. A further support is given by the thermal effect over this temperature range exhibited by rapidly solidified Al–Ni binary alloys in DSC analyses [28, 29]. Because no multi-element phase diagram is available for reference, the simpler alloy systems, of which the present alloy is composed, are utilized. According to the Al–Ni–Si ternary equilibrium phase diagram, a eutecticum (Al–Al_3Ni–Si) at the composition of 5 wt % Ni, 11–12 wt % Si and balance aluminium should be formed in the alloy. Under the rapid solidification conditions as given by air atomization, a certain shift of the ternary eutectic composition can be expected, and a substantial amount of nickel can be assumed to participate in a similar ternary eutectic reaction, especially in the powder particles with medium and large sizes. An Al–Ni phase formed through this reaction can thus be considered to be the major parent phase associated with the large second thermal effect in Fig. 6, if it is still true that there is no Al–Si–Ni ternary compound forming in the Al–Si–Ni eutecticum [13] under the conditions of atomization. With this presumption, previous results obtained from the Al–Ni binary alloys become applicable to the present case, since the crystallographic information on the structure of the meta-stable Al–Ni phase formed in the present powder is not available. Tonejc *et al.* [28] found that in an undercooled hyper-eutectic Al–Ni alloy, the eutectic reaction did not produce the equilibrium phase, Al_3Ni, but an unknown, meta-stable phase which disappeared when the material, having undergone rapid solidification, was annealed at 300 °C for 10 min. This finding was later confirmed [29], and the unknown phase was analysed to be a monoclinic distortion of the orthorhombic unit cell of Al_3Ni. In a similar Al–Ni alloy produced by using droplet emulsion technique with a cooling rate of 500 K s^{-1}, the coexistence of the Al_3Ni and Al_9Ni_2 phases was detected. The later phase, identified from the Al–Fe–Ni system in the absence of iron, coincidentally also had a monoclinic structure, and was decomposed at 375 °C during continuous heating [30]. In the present investigation, X-ray diffractometry revealed that the equilibrium Al_3Ni phase was completely absent in the powder but emerged after the powder was heated at 375 °C. Based on our and other workers' results, it is considered that, in the present atomized powder, the Al_3Ni phase was completely replaced by a distorted, meta-stable phase, perhaps the Al_9Ni_2 phase, as a product of the ternary eutectic reaction under non-equilibrium conditions. The above consideration is yet to be confirmed, but it is certain that the $(AlSi)_7Ni_3$ phase (ASTM 18–44) and $AlSiNi_2$ phase (ASTM 18–43), which are the only Al–Si–Ni ternary compounds existing in the current ASTM cards, were not formed in the atomized powder.

The third large peak centred at 410 °C seems to be related to the precipitation of nickel from the aluminium matrix to form nickel-containing compounds [30]. After the powder was heated and essentially attained its equilibrium state, the X-ray reflections from the Al_3Ni_2 and Al_7Cu_4Ni intermetallic compounds were detected in addition to those from the Al_3Ni phase. The Al_3Ni_2 phase, together with Al_7Cu_4Ni phase, is very likely to be associated with the Al–Cu–Ni system, because it does not exist on the aluminium-rich side of the Al–Ni system or in the aluminium-rich corner of the Al–Si–Ni system [13]. In the Al–Cu–Ni system, copper dissolves in the Al_3Ni_2 phase to form the $Al_3(NiCu)_2$ compound. This is likely also the case in the present alloy upon heating. The reason for this is that copper is practically insoluble in Al_3Ni under the equilibrium conditions (and supposedly also in the meta-stable Al–Ni phase formed during rapid solidification, see above), so that the liquid phase would be enriched in copper, leading to the copper supersaturation in the aluminium matrix during solidification. Upon heating, copper, together with nickel, would precipitate out from the meta-stable aluminium matrix to form $Al_3(NiCu)_2$ and Al_7Cu_4Ni compounds. The formation of the $Al_3(NiCu)_2$ and Al_7Cu_4Ni compounds (named dispersoids hereafter) at such a high temperature confirms a previous finding that nickel substantially reduces the diffusion rate of copper in aluminium [13]. As will be discussed, the formation of these two dispersoids markedly alters the ageing behaviour of the alloy.

It can also be seen from the thermograph (Fig. 6) that during the second and third heating cycles there were no thermal reactions occurring, except the continuing resolution of the alloying elements in the aluminium matrix with rising temperature which gave an endothermic effect. Clearly, after being heated up to 500 °C and slowly cooled in the first run, the powder almost attained its equilibrium condition. Subsequent reheating could only increase the solubilities, mainly of silicon, magnesium and copper, in the aluminium matrix. The silicon crystals and Mg_2Si precipitate, previously formed, were quite possibly redissolved to a certain extent. However, dissolving the $Al_3(NiCu)_2$ and Al_7Cu_4Ni dispersoids, which were the only copper-containing compounds formed, would be difficult during the continuous heating applied in the thermal analysis. The reasons are simply that the diffusion rate of copper in aluminium is reduced by nickel, and the $Al_3(NiCu)_2$ and Al_7Cu_4Ni

dispersoids are known for being thermally stable [13]. This reasoning is supported by the DSC results shown in Fig. 6. The trace of the second heating cycle of the nickel-containing alloy deviates much less from the base line than that exhibited by the base alloy, indicating a decreased amount of resolution as a result of the nickel modification. In this case, the ageing effect in the present alloy given by thermally unstable copper-containing precipitates may be virtually absent. In other words, the addition of nickel to the Al–Si–Cu–Mg base alloy, initially aimed at improving its hot strength and reducing its thermal expansion coefficient, additionally results in a significant modification to its precipitation behaviour. This result was not expected. Apparently, both copper and magnesium were initially desired to form precipitates on ageing. The copper-containing precipitates, the *Q*-phase ($Cu_2Mg_8Si_6Al_5$) and θ-phase ($CuAl_2$), have indeed been observed in the Al–Si–Cu–Mg base alloy [31, 32], and the latter is known to form in a controllable sequence from Guinier–Preston zone, intermediate phase (θ′), finally to equilibrium phase (θ) during ageing [33, 34]. In the alloy with the nickel addition, however, due to the preferred formation of the Al–Ni–Cu dispersoids, a much decreased amount of copper is available to constitute these phases so that little *Q*-phase and θ-phase precipitates can be expected to be formed upon ageing. In this case, only the Mg_2Si phase will be available to create a precipitation strengthening effect. It is well known that in the absence of the *Q*- and θ′-phase precipitates, the Mg_2Si precipitate can only produce medium properties in the Al–Si–Mg system [35]. For the present alloy, the basic strength relies on the dispersions of the silicon crystals, Al_3Ni, $Al_3(NiCu)_2$, and Al_7Cu_4Ni intermetallic compounds as well as on a fine grain structure. The addition to the strength contributed by the Mg_2Si precipitate may only be a very small percentage. A question is thus whether the modified alloy has to be classified as heat treatable, an important point that may not have been recognized by the designers and manufacturers of the alloy. It is predictable that the desired ageing response of the nickel-modified alloy is unlikely to be achievable, in the case that the thermally unstable copper-containing precipitates are absent, and so is a significant improvement of room temperature strength by applying a solid solution and ageing treatment to the final product.

3.3. Microstructural characteristics of individual powder particles

The variations in the as-atomized microstructure with powder particle size, as a result of differing solidification mechanisms, were examined in a large number of powder particles. Shown below is a selection of the microstructures observed from the powder particle sections over a size range corresponding to the most crowded size band (30–160 μm) of the powder (though the section size is not exactly the powder particle size).

Fig. 7a shows a general view of a powder particle section with an elliptical shape and a section size of 40–70 μm, being marginally finer than the measured median size. It is visible in the figure that at the periphery of the powder particle, there are numerous, fine particles with varying sizes, while there are only a few such particles in the interior. Worth noting is that many of these particles are linked to the powder particle surface where a high undercooling and catalysis of solidification by oxides can be expected. Due

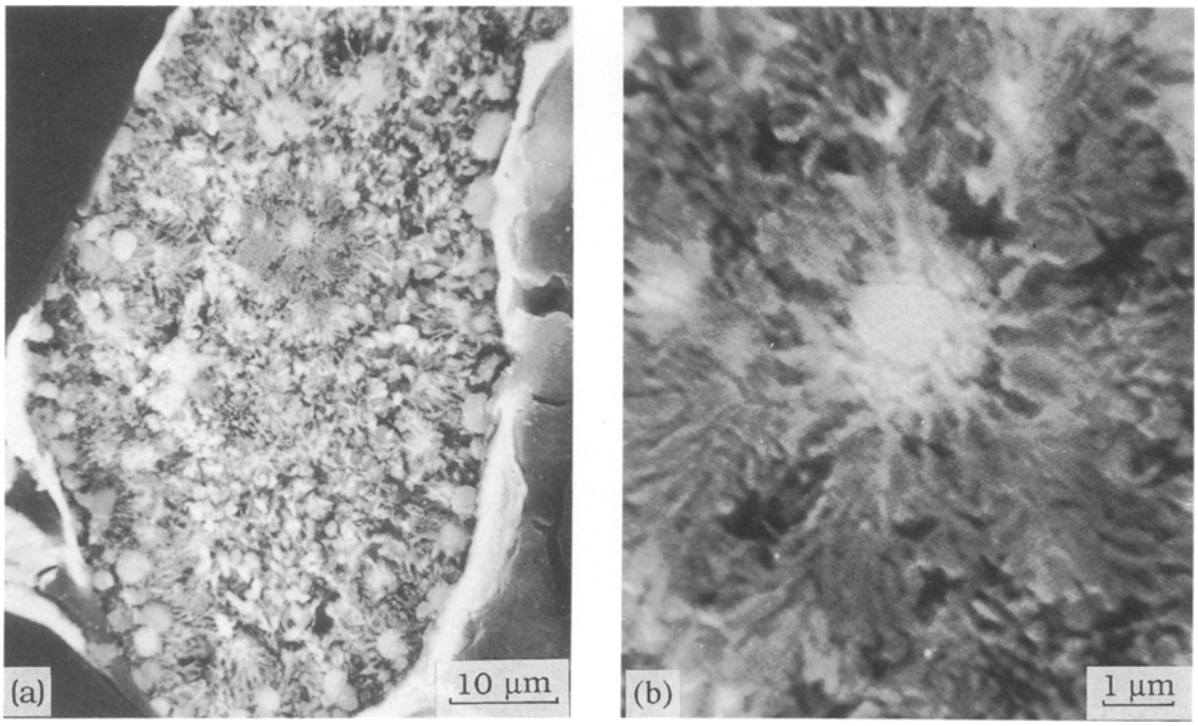

Figure 7 (a) Microstructure of an elliptical powder particle section, and (b) a central solidification core surrounded by a branched eutectic structure.

to their small sizes, direct identification was difficult. Nevertheless, the presumption that they are primarily solidified silicon crystals is unlikely to be tenable, because, in this case, it is difficult to explain why they were much less formed in the interior of the powder particle where a relatively lower undercooling is expected to occur. Moreover, such a presumption is in conflict with the schematic phase diagrams postulated for the rapid solidification of the binary Al–Si and Al–Ni alloys with hyper-eutectic compositions [27, 36]. In line with those diagrams, the solidification processes occurring at the outer rim of the powder particle are as follows. As soon as the atomizing air encountered the liquid stream running out from a nozzle to break it into droplets, oxides were formed on the droplet surfaces. In the mean time, the temperature of the droplets was brought down to a high degree of undercooling, which might be marginally below the coupled eutectic growth region. Owing to the presence of the oxides at the droplet surface, an aluminium based primary phase, which required the least atomic redistributions, was catalysed to form. Its formation decreased the undercooling and brought the temperature of the remaining liquid up to the coupled eutectic region. The above scheme has been proven to be applicable to Al–Si alloys with silicon content below 20 at% [27] and appears to be acceptable for the rapid solidification of the droplet under discussion. From Fig. 7a, a very fine eutectic-like structure radiating from the primary particles can be observed, which means that they acted as nuclei for subsequent coupled growth. Further away from the droplet surface, the extraction of the heat released from the continuing solidification gradually became insufficient to prevent a reduction in undercooling at the growth front. Finally, the local thermal conditions were changed so that the primary silicon crystals enveloped by cells were formed. The formation mechanism of this structure will be discussed later.

The same solidification sequence was, though less frequently, found in the interior of the powder particle. It is easy to locate, in Fig. 7a, a core of solidification from which solidification grew outwards. A close observation revealed that the core is of a size of 1 μm and without the typical morphology of faceted particles (Fig. 7b). The presence of the core at the centre clearly illustrates that the solidification nucleation in the powder particle interior occurred at the early stage of solidification, in addition to that catalysed by the oxides at the surface. In other words, the kinetics of solidification growth initiated at the powder particle surface was not fast enough to cross the entire droplet to prevent other nucleation events. It can be observed from Fig. 7a and b that surrounding the core is a dark grey coloured annulus area with the typical appearance of a eutectic structure. The phases of the eutectic mixture were too fine to be discernible in the SEM in back-scattered electron mode. EDS analysis was also difficult to perform without the disturbing effects of the surroundings. Nevertheless, the knowledge about the phase constituents of the alloy, together with the observation of different etching responses (bright and grey platelets), suggests that the phases in this coupled region are very likely to be the variants of those in the ternary eutecticum (Al–Al_3Ni–Si), possibly Al–Al_9Ni_2–Si, which should be a major eutecticum in the present alloy. The cause for the transition from the core to the coupled eutectic structure can be that the latent heat released from the core solidification could not be transferred out efficiently enough so that the temperature of the growth front was increased into the coupled growth zone. It is clear that the faceted silicon crystals, as commonly observed, are not observable in this area. Outside this annulus area, an equiaxed, cellular structure with internal particles is visible, which meets the same structure growing inwards from the powder particle surface. EDS analysis showed that the internal particles were silicon-rich and surrounded by the aluminium matrix and other intermetallic phases. This transition is again ascribed to an increase in the temperature of the remaining liquid, caused by the latent heat released from the preceding solidification, and an accompanied decrease in thermal gradients, which enabled the direct nucleation of silicon crystals and possibly an Al–Ni intermetallic compound before the coupled growth front. The formation of the primary silicon phase directly from the liquid is clearer in the coarser powder particles, which will be shown later. The stepped transitions from the core outwards through the fine eutectic structure to the formation of coarse, uncoupled phases clearly demonstrate the variations of the thermal conditions at the growth front with the proceeding of solidification in the droplet. This also indicates that the heat flow within a powder particle plays a more important role in determining the solidification mode than the heat extraction to the environment during the solidification initiating at the centre of powder particles.

Not only were microstructural inhomogeneities observed within individual powder particles, but also from one powder particle to another. Fig. 8 shows the as-atomized microstructure of another powder particle section with a round shape and a size of 50 μm, in which multiple nucleation of solidification in the interior in competition with that at the periphery is very evident. As the solidification front grew radially from each core, impingement would occur when the entire droplet was frozen, thus resulting in a flower-like morphology. Although the section size of this powder particle is similar to that shown in Fig. 7, the general morphology is strikingly different, and the size and number of the cores in Fig. 8 are substantially increased. This permitted a reliable spot analysis without the contributions of other phases, which showed that the cores had a chemical composition very close to that of the alloy. There seems to be insufficient evidence to support the hypothesis that the cores with a size of about 4 μm were formed through partitionless solidification in the powder particle produced by air atomization, although such a solidification mechanism was observed to operate in the atomization of other aluminium alloys [37]. In fact, black lines are visible at a very high magnification, as shown in Fig. 8b, which outline a colonial morphology of the cores. These lines appear to be colonial walls which

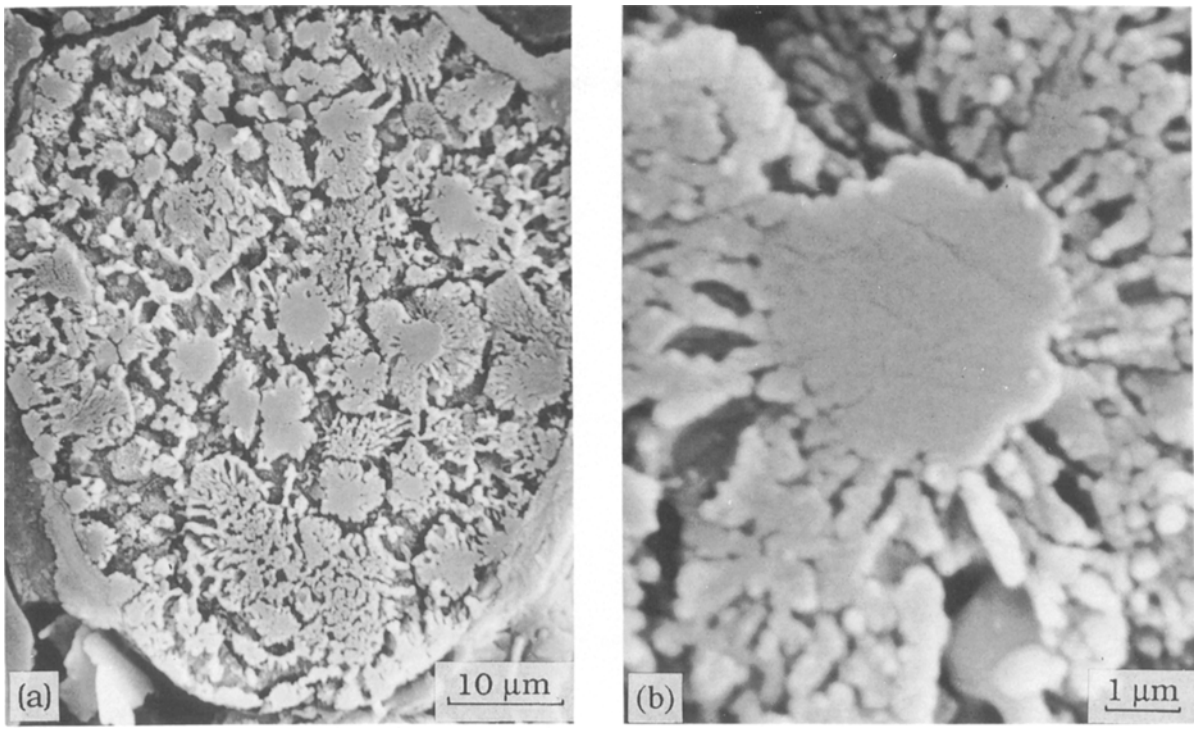

Figure 8 (a) Microstructure of a round powder particle section, and (b) a solidification core and its surroundings.

had a different chemical composition and responded differently to the etchent. It means that segregation occurred to an extent during the core solidification, as a result of the instability of the solidification front. No other features of the cores could be revealed. It is likely that the cores were formed at the initial stage of solidification when the droplets were undercooled well below the extended liquidus. In this case, the formation of the first solid, which required the least atomic redistributions, occurred at potent nucleation sites, such as impurities. This solid would entrap a large amount of alloying atoms to constitute an aluminium based primary phase and to act as cores for subsequent solidification. It has been noted that the cores in the powder particle are not completely segregation free, probably because of the high alloying in the material, which is different from an aluminium alloy with a lower silicon content where the cores formed through segregation-free solidification have been observed by transmission electron microscopy [38].

The increased number of internal solidification cores in Fig. 8a can be understood to be related to the number of active nucleation sites in the droplets, which may have a non-uniform distribution in droplets [39]. The size of the cores depends strongly on the initial undercooling and thermal transfer conditions. A core would grow until the solidification front broke up into the ternary eutectic solidification, as observed in the interior of the powder particle. Fig. 8b shows the structure outside the cores which consists of the branches of silicon phase and aluminium matrix (etched out) decorated with intermetallic phases. The discontinuity in structure from the core to eutectic structure clearly illustrates a transition in solidification mode. It is easy to recognize that this structure is morphologically different from the finely branched eutectic structure shown in Fig. 7b. In Fig. 8b, many branches have been broken up, approaching the typical appearance of an irregular eutectic structure. The difference in the eutectic structure indicates the varying thermal conditions in the individual powder particles.

Fig. 9 shows a powder particle section with a typical tear-drop shape and a size of 25–35 μm, in which the

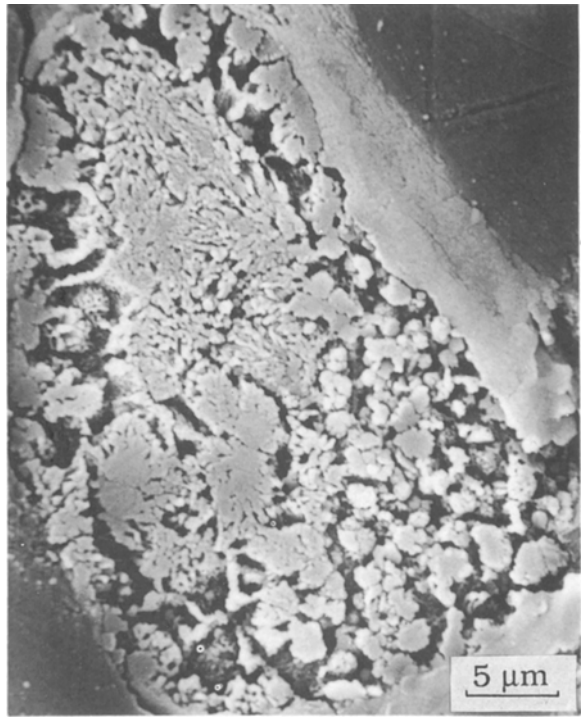

Figure 9 Microstructure of a fine powder particle section with a tear-drop shape.

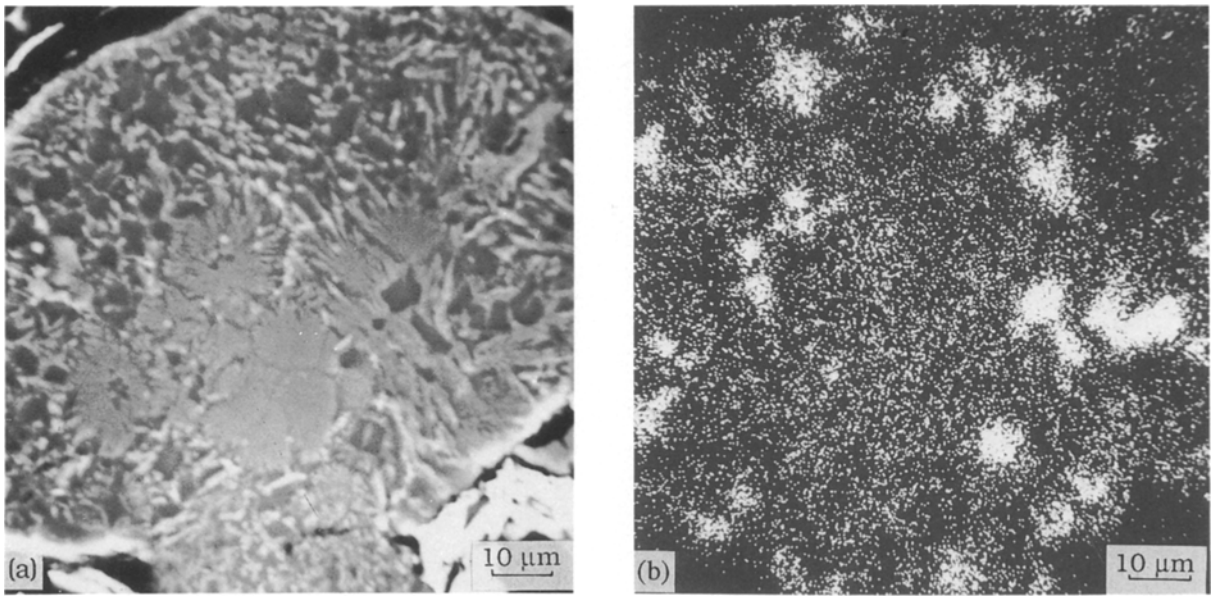

Figure 10 (a) Microstructure of an unetched powder particle section, and (b) distribution of SiK_α on the section.

majority of the section area is composed of the featureless cores and the surrounding eutectic structure. The rest consists of a cellular structure with the internal primary silicon crystals. In this powder particle, transitions are again evident from nucleation at the powder surface and in the meantime in the centre, and then growth in a eutectic manner, to final freezing around the primary silicon crystals. It appears that the lower, thicker part of the droplet solidified last, which reflects the non-uniform undercooling and heat extraction within a powder particle with an irregular shape.

To aid the analysis of the as-solidified structures in the powder particles, X-ray mapping was performed on the powder particle sections without having been etched to observe the distributions of the elements involved in the alloy. From Fig. 10, it is clear that the solidification cores are truly not primary silicon phase, but aluminium based and containing all the alloying elements. The image and SiK_α mapping shown in Fig. 10 were obtained from a large powder particle section so that the primary silicon crystals can clearly be seen. They appear to be concentrated in the middle region between the periphery and the centre, where thermal conditions are in favour of their formation. This is supportive to the above description that the solidification proceeded both inwards and outwards in a droplet. From X-ray mapping, nickel was shown to be homogeneously distributed except being depleted in the silicon-rich areas, but this could be somewhat misleading, because the limited resolution of X-ray mapping might not reveal fine nickel-containing phases in the powder. The bright platelets in Fig. 10 are likely to be an Al–Ni phase which is situated at the branches outside the solidification cores and between the primary silicon crystals, though the exact composition cannot be given by EDS analysis with certainty that the contributions from the neighbouring phases are excluded. It is probable that, in the middle region, solidification started with the formation of the primary silicon crystals and ended with non-equilibrium eutectic reactions in between. No enrichment of copper and magnesium could be found with the limited resolution of X-ray mapping against the refined structures in the rapidly solidified powder, and probably they were entrapped in the matrix and other phases.

For the powder particles with large sizes, the relative section area with the primary silicon crystals was generally increased. Fig. 11a shows a powder particle section with a size of 150 μm, in which the primary silicon crystals are present almost throughout the whole section area. They clearly exhibit a faceted morphological characteristic, as shown in Fig. 11b. Their presence implies that during atomization the undercooling levels attained in the large powder particle could not effectively suppress their extensive formation. The structure between the primary silicon crystals exhibits a low regularity, although there are some morphological characteristics of coupled eutectic lamelae. The association of the primary silicon phase with the rest of the microstructure is not clear (Fig. 11b) and they appear to form independently. For such a large powder particle, the undercooling achievable may be very limited, and moreover the extraction of the heat released from the primary silicon crystal formation cannot be efficient. In this case, a large amount of solutes will be ejected out during the solidification between the primary silicon particles. Obviously, the addition of nickel considerably complicates the solidification of the remaining liquid between the primary particles, which may involve the formation of the meta-stable phases through a combination of Al–Ni–Si and Al–Cu–Ni eutectic reactions modified under non-equilibrium conditions. Post-solidification evolutions in microstructure further prevent the interpretation of the formation mechanisms of the structures between the primary silicon crystals.

The large variations of the as-solidified microstructure within and between the powder particles, presented above, indicate a very high sensitivity of the solidification kinetics to local thermal conditions.

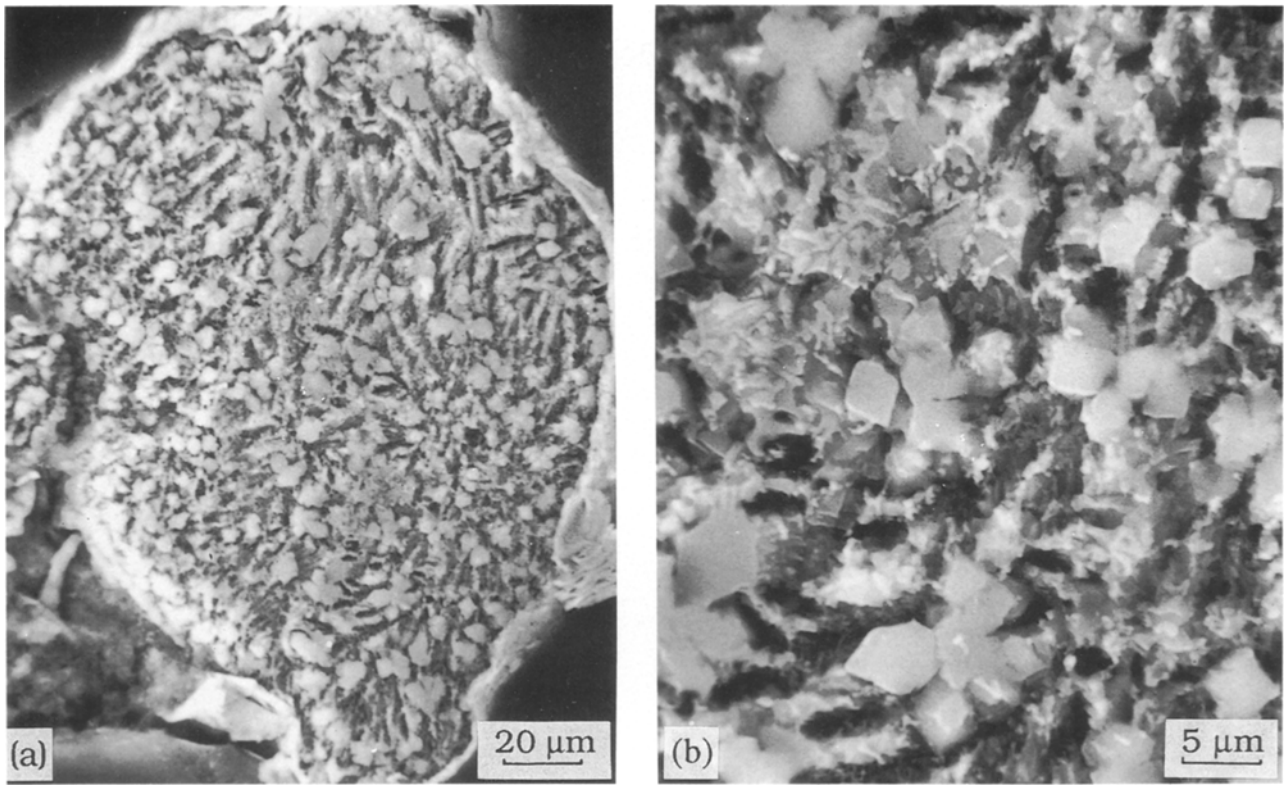

Figure 11 (a) Microstructure of a large powder particle section, and (b) faceted, primary silicon particles surrounded by a complicated structure.

Clearly, the varying powder particle size is principally responsible for the structural inhomogeneities, and non-uniform distributions of undercooling and impurities in the droplets are additional causes. The inhomogeneities observed in the present powder seem to be an inherent characteristic of a complex alloy produced by atomization on a commercial scale. They have been encountered in a number of other atomized aluminium alloys and reported to hamper the achievement of the desired properties of the materials after consolidation [40–42]. It is, therefore, necessary to minimize them by optimizing atomization conditions, though a proper consolidation process by extrusion is instrumental to reducing them, which will be reported in a subsequent communication.

4. Conclusions

1. The air atomized powder exhibited a wide variation of powder particle size and irregular shapes, which have been considered to be closely related to the non-uniformity of undercooling and heat-releasing conditions and thus to be a major cause for the microstructural inhomogeneities of the powder particles.

2. The average lattice parameter of the aluminium matrix in the powder was found to be close to that of pure aluminium, which has been explained by the combined influence of the solute supersaturation and silicon crystals in the material. A broadened diffraction line from the matrix of the powder, was also observed, which has been attributed to the strains caused by the silicon phase and the non-uniformity of the supersaturation. The X-ray reflections from the phases other than the aluminium matrix and silicon phase could not be assigned to any known compounds, indicating the presence of meta-stable phases in the powder.

3. Heating the powder resulted in the decomposition of the meta-stable aluminium matrix and the formation of three nickel-containing intermetallic dispersoids, Al_3Ni, $Al_3(NiCu)_2$ and Al_7Cu_4Ni. These three phases were transformed from the meta-stable phases initially formed in the powder and/or formed through the precipitation from the meta-stable aluminium-rich matrix.

4. The addition of nickel to the Al–Si–Cu–Mg base alloy prevented the formation of the copper-containing precipitates which were initially desired to contribute to the room temperature strength of the material, because of the incorporation of copper in the Al_3Ni_2 phase and the formation of Al_7Cu_4Ni dispersoid. This suggests a significant reduction in the ageing response of the alloy and possibly a change in the alloy category and the processing procedure of the final product.

5. The as-solidified microstructure varied from one powder particle to another, mainly with size. Transitions across each powder particle were also observed, which reflect the changes in solidification mechanism as a function of local thermal conditions. In the medium and fine powder particles, solidification initiation in the interior occurred in addition to that at the periphery. The solidification cores were nearly featureless and aluminium based. They acted as nuclei for subsequent coupled eutectic growth. The growth proceeded until the local thermal conditions could not suppress the formation of the primary silicon phase. In

the coarser powder particles, the primary, faceted silicon phase was extensively formed, and the solidification between the primary silicon crystals was very complicated. The observed significant inhomogeneities in microstructure would affect the properties of the material and should therefore be minimized in powder production and reduced in subsequent processing.

Acknowledgements

The authors are grateful to the Showa Denko K.K., Japan, for providing the powder used in this work. Thanks are also due to Ing. N. M. van der Pers, Drs M. Starink and Ing. E. J. A. van Dam for their help with X-ray diffraction, DSC and SEM analyses, respectively. The financial support of the Programme of Innovative Research (IOP) in the Netherlands is highly appreciated.

References

1. K. AKECHI, Y. ODANI and N. KUROISHI, *Sumitomo Electric Tech. Rev.* **24** (1985) 191.
2. H. M. SKELLY and C. F. DIXON, *Int. J. Powder Metall.* **7** (1971) 47.
3. J. BECKER and G. FISCHER, in Proceedings of the World Conference on Powder Metallurgy, London, July 1990, Vol. 3 (The Institute of Metals, London, 1990) p. 120.
4. H. SANO, K. SHIBUE, S. YAMAUCHI and S. INUMARU, *Sumitomo Light Metal Tech. Rep.* **26** (1985) 215.
5. N. KUROISHI, Y. ODANI and Y. TAKEDA, *Metal Powder Report* **40** (1985) 642.
6. J. ZHOU, J. DUSZCZYK and B. M. KOREVAAR, *J. Mater. Sci.* **26** (1991) 5275.
7. T. HIRANO and T. FUJITA, *J. Jpn Inst. Light Metals* **37** (1987) 670.
8. T. HIRANO, F. OHMI, S. HORIE, F. KIYOTO and T. FUJITA, in Proceedings of the International Conference on Rapidly Solidified Material, San Diego, California, February 1986, edited by P. W. Lee and R. S. Carbonara (ASM, Metals Park, Ohio, 1986) p. 327.
9. K. NAGASAKA, *Nikkei Mechanical* **3** (1989) 44.
10. J. ZHOU, J. DUSZCZYK and B. M. KOREVAAR, *J. Mater. Sci.* **26** (1991) 824.
11. *Idem.*, in Proceedings of the World Conference on Powder Metallurgy, London, July 1990, Vol. 2 (The Institute of Metals, London, 1990) p. 307.
12. *Idem., J. Mater. Sci.* **26** (1991) 3041.
13. L. F. MONLDOFO, in "Aluminium Alloys, Structure and Properties" (Butterworths, London, 1976) p. 604.
14. Y. TAKEDA, Y. ODANI, T. HAYASHI and K. AKECHI, in Proceedings of the World Conference on Powder Metallurgy, London, July 1990, Vol. 1 (The Institute of Metals, London, 1990) p. 392.
15. F. HEHMANN, Y. BIENVENU, M. DURAND, B. MUNAR, U. EILRICH, K. HUMMERT, P. LASNE and C. LEVAILLANT, *ibid.* p. 216.
16. Private Communication, Technical Research Laboratories, Summitomo Light Metal Industries Ltd, Nagóya, Japan, June 1989.
17. J. L. ESTRADA and J. DUSZCZYK, *J. Mater. Sci.* **25** (1990) 886.
18. J. L. ESTRADA, Ph.D. thesis, Delft University of Technology, The Netherlands, 1990.
19. G. H. TAN and T. SHEPPARD, *Powder Metall.* **29** (1986) 143.
20. J. ZHOU, J.DUSZCZYK and B. M. KOREVAAR, *J. Mater. Sci.* **26** (1991) 3292.
21. E. J. MITTEMEIJER, P. VAN MOURIK and Th. H. de KEIJSER, *Phil. Mag.* **43** (1981) 1157.
22. G. J. MARSHALL, E. K. IOANNIDIS and T. SHEPPARD, *Metall. Trans. A* **18A** (1987) 407.
23. R. DELHEZ, Th. H. de KEIJSER, E. J. MITTEMEIJER, P. VAN MOURIK, N. M. VAN DER PERS, L. KATGERMAN and W. E. ZALM, *J. Mater. Sci.* **17** (1982) 2887.
24. N. APAYDIN and R. W. SMITH, *Mater. Sci. Eng.* **98** (1988) 149.
25. M. VAN ROOYEN, Ph.D. thesis, Delft University of Technology, The Netherlands, 1988.
26. I. YAMAUCHI, I. OHNAKA, S. KAWAMOTO and T. FUKUSAKO, in Proceedings of the 5th International Conference on Rapidly Quenched Metals, Würzburg, Germany, September 1984, edited by S. Steeb and H. Warlimont, Vol. 1 (North-Holland, Amsterdam, 1985) p. 1729.
27. K. F. KOBAYASHI and P. H. SHINGU, in Proceedings of the International Conference on Aluminium Alloys – Their Physical and Mechanical Properties, Charlottesville, Virginia, June 1986, edited by E. A. Starke, Jr. and T. H. Sanders, Jr., Vol. 1 (Engineering Materials Advisory Services, Warley, West Midlands, 1986) p. 263.
28. A. TONEJC, D. ROCAK and A. BONEFACIC, *Acta Metall.* **19** (1971) 311.
29. K. CHATTOPADHYAY, P. RAMACHANDRARAO, S. LELE and T. R. ANANTHARAMAN, in Proceedings of the 2nd International Conference on Rapidly Quenched Metals, The Massachusetts Institute of Technology, November 1975, edited by N. J. Grant and B. C. Giesen (The Massachusetts Institute of Technology, Boston, 1976) p. 157.
30. J. H. PEREPEZKO and D. U. FURRER, in Proceedings of a Symposium on Dispersion Strengthened Aluminium Alloys at the 1988 TMS Annual Meeting, Phoenix, Arizona, January 1988, edited by Y. W. Kim and W. M. Griffith (TMS, Warrendale, Pennsylvania, 1988) p. 77.
31. J. ZHOU and J. DUSZCZYK, in Proceedings of the First European Conference on Advanced Materials and Processes, Aachen, Germany, November 1989, edited by E. Exner and V. Schumacher, Vol. 1 (DGM Informationsgesellschaft-Verlag, Oberursel, 1990) p. 241.
32. M. J. STARINK, V. JOORIS and P. VAN MOURIK, to be published in Proceedings of the 1st ASM Heat Treatment and Surface Engineering Conference, Amsterdam, The Netherlands, May 1991.
33. W. BONFIELD and P. K. DATTA, *J. Mater. Sci.* **11** (1976) 1661.
34. S. J. PATERSON and T. SHEPPARD, *Metals Technol.* **9** (1982) 389.
35. D. L. W. COLLINS, *J. Inst. Metals* **86** (1957/58) 325.
36. J. W. ZINDEL, J. T. STANLEY, R. D. FIELD and H. L. FRASER, in Proceedings of an ASTM Symposium on Rapidly Solidified Powder Aluminium Alloys, Philadelphia, April 1984, edited by M. E. Fine and E. A. Starke, Jr. (American Society for Testing and Materials, Philadelphia, 1986) p. 186.
37. T. SHEPPARD and M. A. ZAIDI, *Int. J. Rapid Solidification* **2** (1986) 199.
38. W. J. BOETTINGER, *Mater. Sci. Eng.* **98** (1988) 123.
39. T. SHEPPARD and M. A. ZAIDI, *Mater. Sci. Technol.* **2** (1986) 69.
40. M. A. ZAIDI, *Mater. Sci. Eng.* **98** (1988) 221.
41. E. K. IOANNIDIS, G. J. MARSHALL and T. SHEPPARD, *J. Mater. Sci.* **23** (1988) 1486.
42. M. A. ZAIDI and T. SHEPPARD, *Mater. Sci. Technol.* **3** (1987) 146.

Received 6 March
and accepted 24 April 1991